Geosci. Model Dev. Discuss., 7, 3505–3544, 2014
www.geosci-model-dev-discuss.net/7/3505/2014/
doi:10.5194/gmdd-7-3505-2014

Geoscientific Model Development Discussions
Open Access

A fully coupled 3-D ice-sheet – sea-level model: algorithm and applications

B. de Boer[1,2,*], **P. Stocchi**[3], **and R. S. W. van de Wal**[2]

[1]Department of Earth Sciences, Faculty of Geosciences, Utrecht University, Utrecht, the Netherlands
[2]Institute for Marine and Atmospheric research Utrecht, Utrecht University, Utrecht, the Netherlands
[3]NIOZ Royal Netherlands Institute for Sea Research, Den Burg, Texel, the Netherlands

[*]Invited contribution by B. de Boer, recipient of the EGU Outstanding Student Poster Award 2013.

Received: 7 May 2014 – Accepted: 13 May 2014 – Published: 23 May 2014

Correspondence to: B. de Boer (b.deboer@uu.nl) and P. Stocchi (p.stocchi@nioz.nl))

Published by Copernicus Publications on behalf of the European Geosciences Union.

Abstract

Relative sea-level variations during the late Pleistocene cannot be reconstructed regardless of the estimates of ice-volume fluctuations. For the latter, however, the knowledge of regional and global relative sea-level variations is necessary. Overcoming this problem of circularity demands a fully coupled system where ice sheets and sea level vary consistently in space and time and dynamically affect each other. Here we present results for the past 410 000 years (410 kyr) from the coupling of a set of 3-D ice-sheet-shelf models to a global sea-level model based on the solution of gravitationally self-consistent sea-level equation. The sea-level model incorporates all the Glacial Isostatic Adjustment feedbacks for a Maxwell viscoelastic and rotating Earth model with variable coastlines. Ice volume is computed with four 3-D ice-sheet-shelf models for North America, Eurasia, Greenland and Antarctica. With an inverse approach, ice volume and temperature are derived from a benthic δ^{18}O stacked record. The ice-sheet thickness variations are then forwarded to the sea-level model to compute the bedrock deformation, the geoid and the relative sea-level change. The latter are used to generate the new topographies for the next time step, which are forwarded to the ice-sheet models. To quantify the impact of relative sea-level variations on ice-volume evolution, we have performed coupled and uncoupled simulations. The largest differences of ice-sheet thickness change show up in the proximity of the ice-sheets edges, where relative sea-level change significantly departs from the ocean-averaged sea level variation.

1 Introduction

Periodical expansion and retreat of continental ice sheets has been the main driver of global sea-level fluctuations during the Pleistocene (Fairbridge, 1961). Similarly, deep-sea benthic δ^{18}O records, a proxy for temperature and ice volume, indicate that the volume of the oceans oscillated throughout the last $\sim$ 5.0 Myr in response to global climate changes (Chappell and Shackleton, 1986; Lisiecki and Raymo, 2005). The

separation of the benthic δ^{18}O signal in temperature and ice volume can be deduced by using a combination of ice-sheet models and an air-to-ocean temperature coupling function (de Boer et al., 2013).

The Last Glacial Maximum (LGM, 21.0 kyr ago) is definitely the best studied example of a glacial event during which continental ice sheets covered large portions of North America and Eurasia, and when the ice sheets on Antarctic and Greenland ice sheets extended towards the continental shelf edge (e.g. Ehlers and Gibbard, 2007; Denton et al., 2010). In fact, several well dated surface geological features of depositional and/or erosive origin constrain the maximum LGM ice sheets extent (Ehlers and Gibbard, 2007), and therefore support the ice-sheet volume increase inferred from the benthic δ^{18}O data (Lisiecki and Raymo, 2005). Both deep-sea benthic δ^{18}O records and surface glacial geological features find a counterpart in the −120 to −130 m relative sea-level low stand that was recorded by submerged fossil coral terraces at Barbados (Peltier and Fairbanks, 2006; Austermann et al., 2013), Tahiti (Bard et al., 1996, 2010; Deschamps et al., 2012) and Bonaparte Gulf (Yokoyama et al., 2000). The sea-level rise recorded at these far-field (w.r.t. ice sheets) sites during the last 19 kyr follows the melting of the LGM ice sheets and, consistently with a decrease of benthic δ^{18}O, marks the transition to the current warmer interglacial (Fairbridge, 1961).

Several coeval post LGM paleo-sea-level indicators from different regions are found nowadays at very different elevations above and below the current mean sea level (Pirazzoli, 1987, 1991). In particular, a long term sea-level drop is observed in the proximity of the former LGM ice sheets (Lambeck et al., 1990). Moving slightly away from the formerly glaciated areas the sea-level trend first switches towards a steep rise (Engelhart et al., 2011) and then smoothly changes towards a eustatic-like sea-level rise which is eventually observed at the far-field sites like Barbados and Tahiti (Fairbanks, 1989; Peltier and Fairbanks, 2006; Bard et al., 1996, 2010; Deschamps et al., 2012). This proves that the melting of the LGM ice sheets resulted in regionally varying sea-level changes and that the spatial variability of sea-level change strongly

depends on the distance from the former ice sheets and also on the shape of the ocean basins (Pirazzoli, 1987, 1991).

Following the deglaciation of an ice sheet, the solid Earth rebounds upwards beneath the former glaciated area, while the far-field ocean basins experience subsidence as a consequence of the increasing ocean water loading. Hence, if the ice-sheet thickness variation is the forcing function for the sea-level change, the solid Earth response plays an important role as sea-level change modulator. The occurrence of global sea-level changes during the Holocene and in particular during the last 6000 years (Pirazzoli, 1987, 1991) shows that the solid Earth continued to deform after the LGM ice sheets were completely melted. However, this delayed response implies that the solid Earth behaves like a highly viscous fluid on geological time scales. Indeed, the current vertical land-uplift shown by GPS observations over the formerly glaciated areas of Scandinavia and Hudson Bay imply that the solid Earth is not in an isostatic equilibrium yet (Milne et al., 2001). Importantly, the vertical rebound of the solid Earth contributes to the vertical deformation of the geoid, i.e. the equipotential surface of gravity which coincides with the mean sea level at rest (Milne et al., 2001). In fact, any vertical deformation of the solid Earth behaves like a density anomaly which is reflected in a change of the equipotential surface of gravity.

Moreover, the mean sea surface is also affected by the gravitational pull exerted by the continental ice sheets on the ocean water. During the melting of an ice sheet the ocean volume is increasing, and so is the hypothetical eustatic sea level. The reduction of gravitational pull exerted on the ocean water, due to the smaller ice mass, causes the sea level to drop in front and nearby the ice sheet and to rise more than it would do eustatically far away from the ice sheet. This effect is known as self gravitation (Woodward, 1888), and once merged to the solid Earth deformations contributes to a larger spatial variability of the sea level change. Furthermore we have to consider the rotation of the Earth around its axis. As a consequence, any surface mass displacement, together with the solid Earth and geoidal deformations, triggers a perturbation

of the polar motion which in turn affects redistribution of melt water in the oceans and hence the mean sea surface height.

All the feedbacks described so far determine the complex process known as Glacial-hydro Isostatic Adjustment (GIA) and affect any sea-level change which is dictated by ice-sheets fluctuations (Farrell and Clark, 1976). According to GIA, the sea-level change recorded at any location represents the local response of the solid Earth and of the geoid to the ice-sheet fluctuations and cannot be directly used as representative of the eustatic sea-level change (oceans or ice-sheets volume variation). In fact, since the GIA feedback results in the mutual motion of the solid Earth and of the geoid, any land-based sea-level indicator is eventually a RSL indicator as it records the local variation of the vertical distance between the geoid and the bottom of the ocean.

The GIA feedbacks are usually accounted for by solving the gravitationally self-consistent Sea Level Equation (SLE), which was initially developed by Farrell and Clark (1976), and later on updated to include all the GIA feedbacks (Mitrovica and Peltier, 1991). The SLE describes the global RSL changes, i.e. geoid deformations w.r.t. the centre of mass of the Earth, the solid Earth deformations and consequently the RSL changes for a prescribed ice-sheet chronology and solid Earth rheological model (Spada and Stocchi, 2007). The SLE has been widely employed to improve and refine our knowledge of the LGM ice-sheets volume, thickness and extent and their following deglaciation until the present day (Peltier, 2004).

However, a global ice-sheet model is needed to explain the observed RSL changes, but at the same time the observed RSL changes are needed to refine the global ice-sheet models. This problem of circularity follows from the fact that the ice-sheets evolution is coupled to the RSL changes, which eventually define the variations of the topography and bathymetry. The latter affect the precipitation and the ice-flow pattern. Also, and very importantly, the ice-sheet induced RSL changes affect the portions of marine grounded ice.

Thus far transient simulations of ice sheets have been carried out using global average sea level (Huybrechts, 2002; Zweck and Huybrechts, 2005;

Bintanja and Van de Wal, 2008; Pollard and DeConto, 2009; de Boer et al., 2013). Computational power was limited and the transition from grounded to floating ice-flow in 3-D ice-sheet-shelf models is only adequately accounted for in recent years (Pollard and DeConto, 2009, 2012; Winkelmann et al., 2011; de Boer et al., 2013). There have been no studies that provide a mutually consistent solution of ice volume and regional sea level over longer time scales (Clark et al., 2002; Weber et al., 2011; Raymo and Mitrovica, 2012). Only recently Gomez et al. (2013) have succeeded in coupling a 3-D ice-sheet with a sea-level model for simulating the Antarctic ice sheet from the LGM to the present. The importance of a mutual solution has already been recognised during the mid 1970s affecting the instability of marine terminating ice sheet (Weertman, 1974; Farrell and Clark, 1976). Likewise, sea-level change has a strong influence on the dynamical behaviour of marine ice sheets (e.g. Gomez et al., 2010a, 2013) such as the West Antarctic ice sheet (Pollard and DeConto, 2009). Henceforth, it is of vital importance to incorporate regional sea-level variations when modelling ice-sheets over 10^3–10^6 years.

In this paper we present a system of four regional 3-D ice-sheet-shelf models (de Boer et al., 2013) that is fully dynamically coupled to a global GIA model based on the SLE. Our algorithm represents an alternative method for modelling ice sheets fluctuations and the related GIA induced relative sea-level changes on a global scale. In fact, rather than using a predefined ice-sheet model as forcing function, we build it dynamically on top of a deformable Earth model where crustal and geoidal deformations account for self gravitation, Earth rotation and an adequate treatment of the migration of coastlines. Our new model offers several opportunities to model any ice-sheet and sea-level fluctuation, from the past to the present day and also into the future. Here, we calculate RSL as a function of all ice-sheet volume change over the globe. This allows a comparison with any local record of RSL with a time interval of the past 410 kyr.

2 Methods

In this study we present a new system that is based on the dynamical coupling between (i) ANICE, a fully coupled system of four 3-D regional ice-sheet-shelf models (de Boer et al., 2013) and (ii) SELEN, a global scale sea-level equation model which accounts for all the GIA feedbacks (Spada and Stocchi, 2007). In the following, we first describe separately the ANICE and SELEN sub systems, and consequently introduce the coupling method/algorithm, with particular emphasis on spatial (see Appendix A) and temporal discretisation.

2.1 The ANICE regional ice-sheet-shelf model

The ice-sheet-shelf model used in this framework is a 3-D coupled ice sheet-ice shelf model called ANICE (Bintanja and Van de Wal, 2008; de Boer et al., 2013, 2014). The model is a shallow-ice model, for which we use approximate equations for sheet and shelf flow. These approximations are based on the shallowness of a large ice body, with horizontal scales far larger than the thickness of the ice. In ANICE we apply two approximations, the Shallow Ice Approximation (SIA) (Hutter, 1983) as the basis for land based ice flow and the Shallow Shelf Approximation (SSA) (Morland, 1987) is used for floating ice and sliding velocities (de Boer et al., 2013).

Within this framework we incorporate four separate ice-sheet models for the regions with major ice sheets during the Pleistocene; The Antarctic Ice Sheet (AIS); the Greenland Ice Sheet (GrIS); the North American Ice Sheet (NaIS); and the Eurasian Ice Sheet (EuIS). The models are solved separately on a rectangular x-y grid (see Table 1). Ice temperatures and velocities are solved in three dimensions with 15 grid points in the vertical, which is scaled with ice thickness and has a higher resolution at the bottom, starting with 1 % and increasing to 10 % at the top.

We adopted initial basal and surface topographies for Antarctica from the ALBMAP dataset (Le Brocq et al., 2010) and for Greenland from BEDMAP (Bamber and Layberry, 2001). The initial topography for Eurasia and North America is based on a high

resolution present day (PD) topography dataset (SRTM30_PLUS; Becker et al., 2009). As initial climate forcing we used the PD meteorological conditions from the ERA-40 Re-analysis dataset (Uppala et al., 2005). We calculated monthly averages from 1971 to 2000 for precipitation (in m.w.e.yr^{-1}), 2 m surface-air temperature (°C), and 850 hPa wind fields (in m s^{-1}). The surface topography for the EuIS and NaIS and the ERA-40 climate fields were interpolated on the rectangular ANICE grids with an oblique stereographic projection using the OBLIMAP programme (Reerink et al., 2010).

The uncoupled ice-sheet models ANICE accounts for the bedrock deformation that follows from variations in ice thickness and ocean water by means of a two layer flexural Earth model (Le Meur and Huybrechts, 1996). The upper layer mimics the elastic lithosphere and therefore accounts for the shape of the deformation. The time response of the bedrock deformation is controlled by the lower viscous asthenosphere, with a constant response time of 3 kyr. The rate of the vertical bedrock movement is proportional to the deviation of the profile from the initial equilibrium state and inversely proportional to the relaxation time (Le Meur and Huybrechts, 1996; de Boer et al., 2013). Within the uncoupled ANICE system, eustatic sea-level is calculated from ice-volume changes relative to PD (de Boer et al., 2013, 2014).

2.2 Model forcing

To simulate the evolution of the ice volume through time, we use benthic oxygen isotope δ^{18}O data as input, which is a proxy for changes in ice volume and deep-water temperature (Chappell and Shackleton, 1986). Here, we used the LR04 benthic δ^{18}O stack of 57 deep-sea sediment records (Lisiecki and Raymo, 2005) with an inverse procedure to separate the benthic δ^{18}O data in an ice-volume and deep-water temperature part (de Boer et al., 2013). Since this dataset uses globally distributed records of benthic δ^{18}O data, we assume the record represent a global average climate signal (de Boer et al., 2013). From the benthic δ^{18}O a temperature anomaly relative to PD is derived with an inverse procedure (Bintanja and Van de Wal, 2008; de Boer et al., 2013, 2014). The method is based on the assumption that both ice volume and

deep-water temperature are strongly related to the mid-latitude-to-subpolar Northern Hemisphere (NH) surface-air temperature. This continental mean (40° to 80° N) temperature anomaly controls the waxing and waning of the EuIS and NaIS (Bintanja et al., 2005). The procedure linearly relates the NH temperature to the difference between the modelled and observed benthic δ^{18}O 100 years later, the time resolution of the forcing, given by:

$$\Delta T_{\mathrm{NH}} = \overline{\Delta T_{\mathrm{NH}}} + 20\left[\delta^{18}\mathrm{O}(t) - \delta^{18}\mathrm{O}_{\mathrm{obs}}(t + 100\,\mathrm{yr})\right]. \quad (1)$$

Here, $\overline{\Delta T_{\mathrm{NH}}}$ is the mean NH temperature anomaly over the preceding 2000 years (2 kyr) and the second term on the r.h.s. represent the temperature response to changes in the δ^{18}O record. Furthermore, the modelled benthic δ^{18}O is calculated using ice volume, ice-sheet δ^{18}O and deep-ocean temperatures relative to PD. As a constraint, the modelled benthic δ^{18}O value is determined by minimising the difference between modelled and observed δ^{18}O i.e. the observed δ^{18}O record must be accurately followed (de Boer et al., 2013). The calculated temperature anomaly is forwarded to the ice-sheet models and uniformly added to the surface temperature field. Within each model the surface temperatures are also corrected for surface height changes with a temperature lapse rate. As a result, the model computes ice volume and temperature consistent with the benthic δ^{18}O forcing (Fig. 1). For a full description of ANICE see de Boer et al. (2013).

2.3 The SELEN global sea-level equation model

SELEN solves the SLE by means of the pseudo-spectral method (Mitrovica and Peltier, 1991; Spada and Stocchi, 2007; Stocchi et al., 2013) and retrieves the deformations of the solid Earth (U), of the geoid (N; mean sea surface at rest) and of the relative sea level (S) as function of time on a global scale:

$$S = N - U \quad (2)$$

The two fundamental ingredients within the SLE are (i) the ice-sheet thickness chronology, which represents the forcing function for the sea-level change, and (ii) the solid Earth rheological model, which describes the response of the solid Earth and of the geoid to the melt-water redistribution. The Earth is assumed to be spherically symmetric, self gravitating and radially stratified.

The rheological parameters only depend upon the distance from the centre of mass of the Earth and no lateral variations are accounted for. The outer shell is assumed to be perfectly elastic and mimics the lithosphere. The mantle is discretised into n Maxwell viscoelastic layers (linear rheology) while the inner core is assumed to be inviscid. Our current settings are an elastic lithosphere thickness of 100 km and a $n = 3$ layer Earth model with a viscosity for the shallow upper layer of 3×10^{20} Pa s, a transition zone of 6×10^{20} Pa s and a lower layer of 3×10^{21} Pa s. We adopt the normal modes technique to generate the response of the Earth to variations of surface ice and water loading (Peltier, 1974).

The spatio-temporal variations of ice-sheet thickness represent the a priori forcing function which drives the corresponding self consistent RSL changes. At the core of the SLE is the concept that any local RSL change depends upon any surface mass displacement (both ice and melt water) which has occurred since the beginning of the ice-sheet chronology anywhere on the Earth. Recent improvements account for the dynamical feedback from the solid Earth rotation and the lateral migration of coastlines, also known as the time-dependent ocean function (Milne and Mitrovica, 1998; Mitrovica and Milne, 2003; Kendall et al., 2005). We solve the model with a pseudo-spectral numerical scheme (Spada and Stocchi, 2007) for which we here truncate at a spherical harmonic degree of order 128 to save computation time.

3 The fully coupled system of ANICE and SELEN

Here, we describe the dynamical interaction between the four regional 3-D ice-sheets-shelf models which define the ANICE sub system (see Sect. 2.1), and the

gravitationally self-consistent SLE, which is solved by means of SELEN (see Sect. 2.3) as illustrated in Fig. 2. In the uncoupled ANICE sub system, each regional ice-sheet model deforms its own regional topography independently from the other three ice sheets. Altogether, the four regional ice-sheet models contribute to, as well as respond to, the global eustatic sea-level change, the latter being therefore the only means of connection among the four ice sheets. However, according to the SLE, solid Earth and geoid deformation at each point in space and time linearly depend on all the ice-sheet thickness variations and on the corresponding changes in the ocean loading that have occurred so far. Having ANICE and SELEN fully and dynamically coupled implies that information is exchanged between the two sub systems through time. ANICE feeds SELEN with ice-sheet thickness variation in space and time, while SELEN gives back the corresponding RSL change (representing both variations in U and N, see Eq. 2) to ANICE.

The two means of communication between ANICE and SELEN are the input array IA(λ, θ) which carries information about ice-sheet thickness variation in space, and the output array OA(λ, θ) which retrieves the RSL change at each element of the four ANICE quadrants. Both are a function of latitude (λ) and longitude (θ). The output array is used within ANICE to update the topography for the next time step, which is 1000 years. Before the coupling starts, ANICE is spun up for 1 glacial cycle in the uncoupled mode without SELEN.

3.1 Spatial discretisation

The execution of the algorithm starts with the discretisation of the Earth surface into almost equal-area hexagonal elements. The number of hexagons, i.e. the resolution of the global mesh used within SELEN, depends on the parameter RES (Spada and Stocchi, 2007) (see Appendix A). We hereafter choose a RES value of 60, which provides 141 612 hexagonal elements. Hence, for RES = 60 each element approximately corresponds to a disc with a half amplitude of $\alpha = 0.304$ angular degrees (see Appendix A). We employ the surface interpolation routine grdtrack from GMT (Wessel

and Smith, 1991) to project ETOPO1 topography on the global mesh (Amante and Eakins, 2009). For each element the grdtrack routine provides a value for the bedrock topography as well as a value for the ice elevation which is non zero wherever ice is currently present. Wherever the bedrock height is negative and the ice elevation is non zero, we evaluate whether the ice is grounded or floating. This is essential for defining the ocean function that describes if an element belongs to the ocean or to the land.

Once the initial global topography file is generated, we update this field by projecting the four initial ANICE topographies and ice-sheet thickness. However, the three Northern Hemisphere regional ice-sheets models (NaIS, EuIS and the GrIS) share overlapping regions. We therefore define a hierarchical procedure where the topography and ice-sheet thickness values to be interpolated on the elements are firstly those from the NaIS, then the EuIS and finally the GrIS and AIS (see Supplement). The ANICE grid points and SELEN ice elements are shown in Fig. 3 and total numbers are provided in Table 1.

The geographical coordinates of the elements which are initially updated with the four separate ANICE topographies and ice-sheet thickness are stored in the input array. These are in fact the elements that could potentially be affected by ice-thickness variation through time, and consequently are recognised by SELEN as ice-sheet elements (Fig. 3b and d). The ice-sheet thickness is initially zero in ice free areas and non zero wherever there is currently grounded ice, i.e. on Greenland and Antarctica. Hence, this initial array is the projection of topography and ice thickness of the four ANICE quadrants on the global hexagonal mesh and represents an interglacial stage from which all of our simulations start. Clearly, at each time step of the simulation, the array is updated with new ice-sheet thickness values according to ANICE, and the information is passed to SELEN for the computation of the GIA-induced RSL changes. The latter are then given back to ANICE by means of the output array which stores the geographical coordinates of the centroids of the equal-area elements of the four ice-sheet regions.

3.2 Temporal discretisation

In SELEN, the temporal discretisation is performed assuming that the variables vary stepwise in time (Spada and Stocchi, 2007). Usually, the late Pleistocene ice sheet time histories that are available from literature (e.g. Peltier, 2004) are discretised into time steps of 500 or 1000 years. The ice thickness at a give time represents the height of the ice column until that very time. Provided that the solid Earth behaves like a Maxwell viscoelastic body (see Sect. 2.3), the RSL change induced by the ice thickness variation between two consecutive times accounts for (i) an immediate elastic part which occurs as soon as the second ice-sheet thickness is loaded, and (ii) a following viscous part which depends on the mantle viscosity profile and on the length of the time step Δt_S.

When using SELEN for a prescribed a priori ice-sheet chronology, the spatio-temporal discretisation of ice-sheet thickness is assimilated at once (Spada and Stocchi, 2007). Consequently, given the number and the time step Δt_S, as well as the Load love numbers (Spada et al, 2004), the RSL change is computed by means of spatio-temporal convolutions over the surface of the Earth. Accordingly, the RSL change at any location on the Earth and time since the beginning of the ice-sheet chronology accounts for all the surface ice and ocean load variations that have occurred until that very time (see Sect. 2.3). This implies that, by assuming a predefined mantle viscosity profile, it is possible to compute RSL changes at any time t after the end of the ice-sheet chronology as a consequence of the mantle viscous relaxation, which is an exponentially decaying function of time (Peltier, 1974).

When coupling ANICE to SELEN, a problem arises because the ice thickness variation through time is not known a priori. With respect to any standard SELEN simulation, in fact, ice-sheet thickness variation is only known up until the time SELEN is called by ANICE, which is done with an interval of 1000 years. This implies that any time ANICE calls SELEN to compute the bedrock deformation as well as the sea surface variation for a specific time step $t > 0$ (where $t = 0$ marks the beginning of the simulation), all the

deformations triggered by the previous time steps must be remembered. Hence, any time t SELEN is called, the SLE must be solved starting again from $t = 0$ (first ice thickness change). As a consequence, the arrays carrying the SLE results grow throughout the simulations. This is not a big problem when simulating short ice-sheets fluctuations like the post LGM melting, but is definitely a limitation when simulating multiple glacial cycles.

To avoid this problem we take advantage of the linearity of both the SLE and of the rheological model. In particular, we use the fact that the viscous response of the bedrock deformation exponentially decays with time and ceases once the isostatic equilibrium has been reached. Accordingly, for the viscous relaxation of the solid Earth that follows, any ice-sheet thickness variation $I(t)$ the RSL changes are evaluated with SELEN at several points in time between $t = \Delta t_S$ and a predefined $t = L$, which is the total length (in kyr) of the memory array. The memory array is consequently updated at any call from ANICE to store the contributions of each ice-sheet thickness variation simulated with ANICE since the initial time step $t = 0$ for every 1000 years (Fig. 2).

At any time t, when ANICE calls SELEN, the bedrock deformation $U(t)$ and the geoid change $N(t)$ due to the ice thickness variation $I(t) = H(t) - H(t-1)$, are computed for a series of consecutive time steps into the future, i.e., for some L thousands of years after t has occurred. Figure 4 illustrates this process for a 20 m of ice that is added at time $t = 0$ (inset of Fig. 4a; using a schematic setup as shown in Fig. 5). SELEN computes the bedrock deformation from $t = 0$ to $t = L$, for which we use $L = 80$ kyr. The bedrock deformation is computed at NT = 15 times in the future. The time steps are heterogeneous, i.e. 10 steps of 1 kyr, 2 steps of 5 kyr and 3 steps of 20 kyr. The black squares show the predicted bedrock deformation at each time step. Then, the bedrock deformation is interpolated within the longer time steps to have a discretised solution at the time step of SELEN $\Delta t_S = 1$ kyr (Fig. 4b). The second time ANICE calls SELEN, another 20 m of ice is added above the initial ice layer, and the bedrock deformation due to this extra mass is computed again in the same way. Then, the new array is summed to the previous one to incorporate the viscous deformations of the initial ice-thickness

variation (Fig. 4c). This process is carried on throughout the whole simulations so that the memory of previous ice thickness variations is maintained (see Fig. 6).

Henceforth, two auxiliary arrays AS(λ,θ,t) and AOF(λ,θ,t) are generated to store the following L kyr of RSL changes and ocean function variations, respectively. Both according to the ice and water loading at time t and both discretised into NT time steps. At the end of each iterative step of the SLE, the ocean functions are updated by overlapping the RSL changes that are induced by the most recent ice-sheet thickness variation, with the previous ones that were stored in the AS(λ,θ,t) array (Fig. 6). This is necessary to account for the variation of coastlines. Accordingly, the output array OA(λ,θ) that is sent back to ANICE only stores the RSL change for the actual time step, $S(\lambda,\theta,1)$. Throughout a full ANICE-SELEN simulation, therefore, the role of the auxiliary arrays AS(λ,θ,t) and AOF(λ,θ,t) is to account for the response to past ice-sheet thickness variations. This avoids the computationally expensive problem of performing, at any call from ANICE, a full temporal convolution since time t = 0.

We call this temporal discretisation scheme the "moving time window". The length of the moving time window L, i.e. how far into the future SELEN solves for the RSL change, is a free parameter. The longer the moving time window, the more accurate the results will be, since more information from the past is taken into account. In order to maintain a long enough moving time window and to save CPU time, it is important to consider the number of discrete time steps NT which define the moving window. If the length of the moving window allows for a longer memory, the number of time steps allow for an accurate discretisation of the RSL change.

4 Results

4.1 Schematic test with the moving time window

As described in Sect. 3.2, SELEN is called by ANICE every 1000 years. Henceforth the length of the moving window L and the length of the time step within SELEN,

Δt_S, must be multiples of the coupling interval. Here, we use a heterogeneous set of time steps NT to include past variations of GIA. To demonstrate the moving time window, we have used an axisymmetric land/ocean configuration that consists of 2 polar continents, separated by a homogeneous ocean (Fig. 5). The coastlines are fixed and an axisymmetric ice load is located on the south pole with a cylindrical shape and a linear varying ice thickness as shown in Fig. 7b. Since the evolution of ice loading is know a priori we can easily solve the standard SLE solution, for which one complete convolution of the SLE is needed over all time steps of the 480 kyr run. These results are then used as a reference solution for the moving-time window experiments.

We have run a series of simulations to test the accuracy of the moving-window technique with using a linear temporal interpolation between the heterogeneous time steps of the moving window. The moving window here covers the entire length of the simulation, but it is made out of NT = 15 time steps. The first 10 steps ΔT_S are 1 kyr long and thereafter 5 heterogeneous steps until 480 kyr. Between these time steps, the GIA signal is linearly interpolation in time (similar to Fig. 4b). Figure 7a shows the normalised residual of the RSL change computed with the moving-time window. We have computed this as:

$$\text{NormRes} = (S_{\text{mw}} - S_{\text{full}})/(S_{\text{full}}) \quad (3)$$

Clearly the largest differences between the moving window method and the standard SLE are located close to the ice sheet and in particular on top of the fore bulge area (Fig. 7a). Here the GIA signal is in fact more complicated than in the ice-covered area and in the far-field sites because of the lithosphere flexural response. For the fully coupled experiments we used an empirical derived window of L = 80 kyr with NT = 15, which is chosen as a trade off between including sufficient memory of the deformation of the solid earth and computational time of the full 410 kyr run.

4.2 Coupled simulations

Our simulations with the coupled ANICE-SELEN system provide variations of regional sea-level through time (see Supplement Movie). As we show in Fig. 8a, RSL varies significantly between different locations and can be quite different from the eustatic (Fig. 8b). For the far field site (Red Sea), the RSL is quite similar to the eustatic curve (black shading), although values are a bit higher. The most striking difference with respect to the eustatic is the Antarctic peninsula. Here, the changes are always higher than PD. Difference in RSL can go up to 100 m, for example between East coast USA (green) and West Europe (blue), which are both relatively close to the large ice sheets on the NH. In particular the largest deviations from the eustatic occur during glacial maxima (Fig. 8b). Moreover, during interglacials local peak values are higher than eustatic. These local differences can thus be large and are important for model-data comparison on a regional scale.

4.3 Comparison with the eustatic solution

The initial setup of the ANICE model as described in de Boer et al. (2013) calculates the change in sea level from the eustatic contributions of the four ice sheets relative to PD. In Fig. 1b, the four contributions of the ice sheets are shown over the 410 kyr time period. Clearly, the largest contributions arise from the NH ice sheets on Eurasia and North America. When we include the regional sea-level variations the local evolution of ice thickness will obviously change due to the self-gravitation effects, especially for the marine parts of the ice sheets.

In Fig. 9 we compare the volume of the modelled ice sheets by ANICE for a run with and without coupling to SELEN over the last glacial cycle. The largest differences occur during the glacial periods, especially for the AIS (Fig. 9a). For Antarctica, these differences are mainly observed in the marine sectors of the ice sheet, i.e. West Antarctica. Here, including the gravitationally self-consistent sea-level change reduced the growth of the ice sheet relative to the non-coupled run. Henceforth, with only eustatic variations

(dashed line in Fig. 9a) the ice sheet grows significantly larger during a glacial period. This self-stabilisation mechanism has been identified before in coupled model simulations for Antarctica by Gomez et al. (2013).

The gravitationally self-consistent solution of SELEN also provides a much more realistic behaviour of the response of the solid Earth to ice- and water-loading. Including the viscoelastic Earth model accounts for the response on multiple time scales and provides a global solution, whereas we use a single time scale (of 3 kyr) response in the uncoupled solution. For all four ice sheets (Fig. 9a–d), our current setup of SELEN provides a lower response of the bedrock relative to the two layer flexural Earth model. Henceforth, especially for the NaIS, this results in a lower total ice volume for the coupled solution (Fig. 9d). Since the coupled simulation takes into account the change of the coastline over the globe (i.e. the time dependent ocean function), the area of the total ocean is reduced by about 7 % during the LGM (Fig. 9e). Consequently, the total eustatic sea level change of the two simulations (Fig. 9f) is coincidently quite similar over the last glacial cycle.

4.4 Rotational feedback

An important aspect of the gravitationally self-consistent sea level is the rotational feedback, which is a new feature in SELEN. The changes in the mass distribution of ice and water induce a shift in the position of the rotational axis (polar wander) that has a ellipsoidal from (e.g. Gomez et al., 2010b). The difference as shown in Fig. 10b is described by the spherical harmonics of degree 2 (e.g. Mound and Mitrovica, 1998) (see also the Supplement Movie). As is shown in Fig. 10b, the positive contribution of the degree 2 signal is centred in the North Atlantic ocean related to the large increase in ice volume in the NH, which thus adds several meters to the drop in sea level during the LGM. In response to these regional differences, local ice thicknesses are different (Fig. 10d), but do not lead to a large difference in total ice volume. However, for the interpretation of regional sea-level data, the addition of the rotation feedback is a significant contribution to the RSL change that can be up to 5 m or higher (Fig. 10b). In addition, there is

a clear dynamical response of the ice sheets (Fig. 10d) to the differences in RSL, which result in a large and significant changes in local RSL values close to the ice sheets.

5 Discussion and conclusions

In this paper we have presented a new algorithm to fully and dynamically couple a 3-D ice-sheet-shelf model (de Boer et al., 2013, 2014) to a Glacial Isostatic Adjustment model based on the Sea Level Equation (Spada and Stocchi, 2007). The two key aspects are the spatial discretisation and related interpolation of the ice volume from four different regional ice-sheet models, and the temporal discretisation scheme with the related time-interpolation. This system is the first fully coupled global ice-sheet – sea-level model available. Here, we have provided a simultaneous simulation of global solution of ice-volume and relative sea-level variations over the past four glacial cycles.

The key aspect of our results is the dynamical response of the ice sheets to changes in RSL, which includes both the deformation of the bedrock to ice and water loading and the geoidal deformations. Due to the self-gravitational pull of the ice sheet, RSL close to the ice sheets is higher than the eustatic sea level and thus acts to stabilise the ice sheets, as has also been shown by Gomez et al. (2013) with a coupled ice-sheet – sea-level model for Antarctica. Henceforth, especially for the AIS, ice volume is lower during glacial periods relative to the uncoupled simulations shown here. Overall the coupled model results in lower ice volume relative to an uncoupled simulation that uses eustatic sea level derived from ice-volume changes only. We also include a time dependent ocean function that accounts for the changes in the coastlines over the globe. This leads to a significant reduction of the ocean area during glacial maxima and hence results in a nearly equal eustatic sea-level change compared to the uncoupled simulations.

The use of the Maxwell viscoelastic Earth model gives a lower response in bedrock deformation due to the ice loading relative to the simplified model used in earlier studies (de Boer et al., 2013). However, we only used a single setup of the model here, whereas

several studies clearly shown the apparent influence of varying the 1-D structure of the Earth model (e.g. Stocchi et al., 2013; Whitehouse et al., 2012a), which is a simplified version of the complex 3-D Earth structure in itself (van der Wal et al., 2013). Additionally, ice-sheet model parameters are not fully constrained either, whereas the mass balance parameterisation we use in ANICE (see de Boer et al., 2013) can be tested within a certain range of physical parameters (e.g. Fitzgerald et al., 2012). Similarly, ice flow and basal sliding can be varied as well (e.g. Maris et al., 2014). In a future study we will investigate the parameter space for both the Earth and ice-sheet models, and comparing with observational data (see for example Whitehouse et al., 2012b; Briggs et al., 2013) on a global scale (Tushingham and Peltier, 1992).

We presented here a complete dynamic system that simulates ice volume and relative sea level on a global scale over multiple glacial cycles. Although the eustatic change in sea level is still a distinct signal for far field sites, regional differences are substantial. Our simulations show that especially during periods with either very high (interglacials) or very low (glacial maxima) sea level relative to PD, local differences can be very large, thus showing the importance of this coupled system for model-data comparison on a regional scale.

Appendix A: Spatial discretisation of SELEN

The SLE requires a global discretisation of both the surface ice–loads (and consequently of the oceanic counterpart, i.e., melt water loading), topography and bathymetry. Therefore, it is necessary to merge the four separate quadrants of ANICE into a global field. Following Spada and Stocchi (2007), we first generate an initial global mask discretised into equal-area hexagonal elements (i.e. pixels). The number of pixels (NP), which defines the resolution of the mask, depends on the parameter RES (Spada and Stocchi, 2007):

$$NP = 2 \times RES \times (RES - 1) \times 20 + 12. \quad \text{(A1)}$$

In this paper we set RES = 60, which results in 141 612 pixels. We plot on this mask the values of topography (both for bedrock and ice elevation) from the high resolution ETOPO1 model (Amante and Eakins, 2009). For this purpose the ETOPO1 topographic values are first interpolated on a global 0.1°×0.1° rectangular grid. Each element is then transformed to an equivalent–area spherical cap of radius α:

$$\alpha(\lambda,\theta) = \arccos\left[1 - \sin(90-\lambda) \times \sin\frac{\beta}{2} \times \frac{\beta}{180}\right], \quad \text{(A2)}$$

where $\beta = 0.1^{\circ}$. At the same manner, the NP pixels of the global mesh are converted into equal area spherical caps of radius:

$$\alpha_{\text{sle}} = (180/\pi) \times \sqrt{4/\text{NP}}. \quad \text{(A3)}$$

With RES = 60, the radius for the global mesh is $\alpha_{\text{sle}} = 0.3$. To assign at each pixel a value that corresponds to the ETOPO1 topography, we evaluate the intersections between the pixels and the disk elements from the ETOPO1 conversion. For this purpose we employ the method described by Tovchigrechko and Vakser (2001). For each pixel, we sum positive (above mean sea level, i.e. land) and negative (below mean sea level, i.e. sea bottom) volumes, using a weighted average. The same is done for the grounded ice. To check if the ice point is still grounded, we evaluate whether the topography is positive or negative. At first, despite the thickness of the ice the pixel is considered land, and a value of 0 is assigned to the label OF. If the topography is negative, we compare the thickness of the ice with the absolute value of bathymetry, considering the density ratio between ice and water, we evaluate if the ice is grounded or floating. As a result, we generate a global topography/bathymetry file based on the original ETOPO1 (Amante and Eakins, 2009). For each pixel the following values are assigned: longitude, latitude, longitude anchor, latitude anchor, ocean function (OF) label, topography, ice thickness label and ice thickness (see Table 2). Furthermore, it is important to bear in mind that according to this discretisation, lakes, ponds and

enclosed basins are considered as part of the (global) ocean function. It is up to the user to design specific masks to remove or add areas to the ocean function.

The global topography must now be updated for the four regions considered by ANICE (North America, Eurasia, Greenland and Antarctica). Of course there are overlapping regions. This is done in a sequential order, starting from North America, then Eurasia, then Greenland and finally Antarctica (see Supplement). For converting the ice thickness on the rectangular grid points of ANICE on to the SELEN pixels we account for conservation of ice volume for each grid point. Similar to the initial topography from ETOPO1, the rectangular grid points are first converted into discs with radius:

$$\alpha_{\text{ice}} = \frac{\Delta x}{R_{\text{E}}\sqrt{\pi}}, \quad \text{(A4)}$$

with the radius of the Earth $R_{\text{E}} = 6371.221$ km. Firstly, the total overlapping area of each ANICE grid point is calculated for all SELEN elements. Secondly, the total volume for each ice covered SELEN element is corrected for the corresponding volume on the (original) ANICE rectangular grid point. Lastly, the interpolated ice thickness is calculated from the volume divided by the area of the SELEN element. This routine is included as Supplement.

Author contributions

The model code was developed by B. de Boer and P. Stocchi, coupled simulations were performed by B. de Boer, P. Stocchi performed the time window tests. B. de Boer and P. Stocchi contributed equally to this manuscript. All authors contributed to the discussion of the results and implications and commented on the manuscript at all stages.

The Supplement related to this article is available online at doi:10.5194/gmdd-7-3505-2014-supplement.

Acknowledgements. Part of this work was supported by COST Action ES0701 “Improved constraints on models of Glacial Isostatic Adjustment”. DynaQlim. NWO. Financial support for B. de Boer was provided through the Royal Netherlands Academy of Arts and Sciences (KNAW) professorship of J. Oerlemans and NWO VICI grant of L. J. Lourens. Model runs were performed on the LISA Computer Cluster, we would like to acknowledge SurfSARA Computing and Networking Services for their support.

References

Amante, C. and Eakins, B. W.: ETOPO1 1 Arc-Minute Global Relief Model: Procedures, Data Sources and Analysis, NOAA Technical Memorandum NESDIS NGDC-24, p. 19, 2009. 3516, 3525

Austermann, J., Mitrovica, J. X., Latychev, K., and Milne, G. A.: Barbados-based estimate of ice volume at Last Glacial Maximum affected by subducted plate, Nat. Geosci., 7, 553–557, 2013. 3507

Bamber, J. L. and Layberry, R. L.: A new ice thickness and bed data set for the Greenland ice sheet 1. Measurements, data reduction, and errors, J. Geophys. Res., 106, 33773–33780 2001. 3511

Bard, E., Hamelin, B., and Fairbanks, R.: Deglacial sea-level record from Tahiti corals and the timing of global meltwater discharge, Nature, 382, 241–244, 1996. 3507

Bard, E., Hamelin, B., and Delanghe-Sabatier, D.: Meltwater pulse 1B and Younger Dryas sea levels revisited with boreholes at Tahiti, Deglacial, 327, 1235–1237, 2010. 3507

Becker, J. J., Sandwell, D. T., Smith, W. H. F., Braud, J., Binder, B., Depner, J., Fabre, D., Factor, J., Ingalls, S., Kim, S.-H., Ladner, R., Marks, K., Nelson, S., Pharaoh, A., Trimmer, R., Von Rosenberg, J., Wallace, G., and Weatherall, P.: Global bathymetry and elevation data at 30 arc seconds resolution: SRTM30_PLUS, Mar. Geod., 32, 355–371, 2009. 3512

Bintanja, R. and Van de Wal, R. S. W.: North American ice-sheet dynamics and the onset of 100 000-year glacial cycles, Nature, 454, 869–872, 2008. 3510, 3511, 3512

Bintanja, R., Van de Wal, R. S. W., and Oerlemans, J.: Modelled atmospheric temperatures and global sea level over the past million years, Nature, 437, 125–128, 2005. 3513

Briggs, R., Pollard, D., and Tarasov, L.: A glacial systems model configured for large ensemble analysis of Antarctic deglaciation, The Cryosphere, 7, 1949–1970, doi:10.5194/tc-7-1949-2013, 2013. 3524

Chappell, J. and Shackleton, N. J.: Oxygen isotopes and sea level, Nature, 324, 137–140, 1986. 3506, 3512

Clark, P. U., Mitrovica, J. X., Milne, G. A., and Tamisiea, M. E.: Sea-level fingerprinting as a direct test for the source of global meltwater pulse IA, Science, 295, 2438–2441, 2002. 3510

de Boer, B., van de Wal, R. S. W., Lourens, L. J., and Bintanja, R.: A continuous simulation of global ice volume over the past 1 million years with 3-D ice-sheet models, Clym. Dynam., 41, 1365–1384, 2013. 3507, 3510, 3511, 3512, 3513, 3521, 3523, 3524

de Boer, B., Lourens, L. J., and van de Wal, R. S. W.: Persistent 400 000-year variability of Antarctic ice volume and the carbon-cycle is revealed throughout the Plio-Pleistocene, Nat. Commun., 5, 2999, doi:10.1038/ncomms3999, 2014. 3511, 3512, 3523, 3535, 3543

Denton, G. H., Anderson, R. F., Toggweiler, J. R., Edwards, R. L., Schaefer, J. M., and Putnam, A. E.: The Last Glacial termination, Science, 328, 1652–1656, 2010. 3507

Deschamps, P., Durand, N., Bard, E., Hamelin, B., Camoin, G., Thomas, A. L., Henderson, G. M., Okuno, J., and Yokoyama, Y.: Ice-sheet collapse and sea-level rise at the Bolling warming 14 600 years ago, Nature, 483, 559–564, 2012. 3507

Ehlers, J. and Gibbard, P. L.: The extent and chronology of Cenozoic global glaciation, Quaternary Int., 164–165, 6–20, 2007. 3507

Engelhart, S., Peltier, W., and Horton, B.: Holocene relative sea–level changes and glacial isostatic adjustment of the US Atlantic coast, Geology, 39, 751–754, 2011. 3507

Fairbanks, R. G.: A 17000 year glacio–eustatic sea–level record: Influence of glacial melting rates on the Younger Dryas event and deep ocean circulation, Nature, 342, 637–642, 1989. 3507

Fairbridge, R. W.: Eustatic changes in sea level, Phys. Chem. Earth, 5, 99–185, 1961. 3506, 3507

Farrell, W. E. and Clark, J. A.: On postglacial sea level, Geophys. J. Roy. Astr. S., 46, 647–667, 1976. 3509, 3510

Fitzgerald, P. W., Bamber, J. L., Ridley, J. K., and Rougier, J. C.: Exploration of parametric uncertainty in a surface mass balance model applied to the Greenland ice sheet, J. Geophys. Res., 117, F01021, doi:10.1029/2011/JF002067, 2012. 3524

Gomez, N., Mitrovica, J. X., Huybers, P., and Clark, P. U.: Sea level as a stabilizing factor for marine-ice-sheet grounding lines, Nat. Geosci., 3, 850–853, 2010a. 3510
Gomez, N., Mitrovica, J. X., Tamisiea, M. E., and Clark, P. U.: A new projection of sea level change in response to collapse of marine sectors of the Antarctic Ice Sheet, Geophys. J. Int., 180, 623–634, 2010b. 3522
Gomez, N., Pollard, D., and Mitrovica, J. X.: A 3-D coupled ice sheet–sea level model applied to Antarctica through the last 40 ky, Earth Planet. Sc. Lett., 384, 88–99, 2013. 3510, 3522, 3523
Hutter, L.: Theoretical Glaciology, D. Reidel, Dordrecht, 1983. 3511
Huybrechts, P.: Sea-level changes at the LGM from ice-dynamic reconstructions of the Greenland and Antarctic ice sheets during the glacial cycles, Quaternary Sci. Rev., 21, 203–231, 2002. 3509
Kendall, R. A., Mitrovica, J. X., and Milne, G. A.: On post-glacial sea level – II. Numerical formulation and comparative results on spherically symmetric models, Geophys. J. Int., 161, 679–706, 2005. 3514
Lambeck, K., Johnston, P., and Nakada, M.: Holocene glacial rebound and sea-level change in NW Europe, Geophys. J. Int., 103, 451–468, 1990. 3507
Le Brocq, A. M., Payne, A. J., and Vieli, A.: An improved Antarctic dataset for high resolution numerical ice sheet models (ALBMAP v1), Earth Syst. Sci. Data, 2, 247–260, doi:10.5194/essd-2-247-2010, 2010. 3511
Le Meur, E. and Huybrechts, P.: A comparision of different ways of dealing with isostacy: examples from modelling the Antarctic ice sheet during the last glacial cycle, Ann. Glaciol., 23, 309–317, 1996. 3512
Lisiecki, L. and Raymo, M.: A Pliocene–Pleistocene stack of 57 globally distributed benthic δ^{18}O records, Paleoceanography, 20, PA1003, doi:10.1029/2004PA001071, 2005. 3506, 3507, 3512, 3535
Maris, M. N. A., Ligtenberg, S. R. M., Crucifix, M., de Boer, B., and Oerlemans, J.: Modelling the evolution of the Antarctic Ice Sheet since the last interglacial, The Cryosphere Discuss., 8, 85–120, doi:10.5194/tcd-8-85-2014, 2014. 3524
Milne, G. and Mitrovica, J.: Postglacial sea-level change on a rotating Earth, Geophys. J. Int., 133, 1–10, 1998. 3514

Milne, G., Davis, J., Mitrovica, J., Scherneck, H., Johansson, J., Vermeer, M., and Koivula, H.: Space-geodetic constraints on glacial isostatic adjustment in fennoscandia, Science, 291, 2381–2385, 2001. 3508
Mitrovica, J. and Milne, G.: On post-glacial sea level: I. General theory, Geophys. J. Int., 154, 253–267, 2003. 3514
Mitrovica, J. X. and Peltier, W. R.: On post–glacial geoid subsidence over the equatorial ocean, J. Geophys. Res., 96, 20053–20071, 1991. 3509, 3513
Morland, L. W.: Unconfined ice-shelf flow, in: Dynamics of the West Antarctic Ice Sheet, edited by: de Veen, C. J. V. and Oerlemans, J., D. Reidel, 99–116, 1987. 3511
Mound, J. E. and Mitrovica, J. X.: True polar wander as a mechanism for second-order sea-level variations, Science, 279, 534–537, 1998. 3522
Peltier, W. R.: Global Glacial isostasy and the surface of the ice-age Earth: the ICE-5G (VM2) model and GRACE, Annu. Rev. Earth Pl. Sc., 32, 111–149, 2004. 3509, 3517
Peltier, W. R.: The impulse response of a Maxwell Earth, Rev. Geophys. Space Ge., 12, 649–669, 1974. 3514, 3517
Peltier, W. R. and Fairbanks, R. G.: Global glacial ice volume and Last Glacial Maximum duration from an extended Barbados sea level record, Quaternary Sci. Rev., 25, 3322–3337, 2006. 3507
Pirazzoli, P. A.: Sea-level changes in the Mediterranean, in: Sea-Level Changes, edited by: Tooley, M. J. and Shennan, I., Blackwell, Inst. British Geogr. Spec. Publ. Ser. 20, 152–181, 1987. 3507, 3508
Pirazzoli, P. A.: World Atlas of Holocene Sea Level Changes, Elsevier, Amsterdam, 300 pp., 1991. 3507, 3508
Pollard, D. and DeConto, R. M.: Modelling West Antarctic ice sheet growth and collapse through the past five million years, Nature, 458, 329–332, 2009. 3510
Pollard, D. and DeConto, R. M.: Description of a hybrid ice sheet-shelf model, and application to Antarctica, Geosci. Model Dev., 5, 1273–1295, doi:10.5194/gmd-5-1273-2012, 2012. 3510
Raymo, M. E. and Mitrovica, J. X.: Collapse of polar ice sheets during the stage 11 interglacial, Nature, 483, 453–456, 2012. 3510
Reerink, T. J., Kliphuis, M. A., and van de Wal, R. S. W.: Mapping technique of climate fields between GCM's and ice models, Geosci. Model Dev., 3, 13–41, doi:10.5194/gmd-3-13-2010, 2010. 3512

Spada, G. and Stocchi, P.: SELEN: A Fortran 90 program for solving the “sea-level equation”, Comput. Geosci., 33, 538–562, 2007. 3509, 3511, 3513, 3514, 3515, 3517, 3523, 3524

Spada, G., Antonioli, A., Boschi, L., Cianetti, S., Galvani, G., Giunchi, C., Perniola, B., Piana Agostinetti, N., Piersanti, A., and Stocchi, P.: Modeling Earth’s post–glacial rebound, EOS, Transactions, American Geophysical Union, 85, 62–64, 2004. 3517

Stocchi, P., Escutia, C., Houben, A. J. P., Vermeersen, B. L. A., Bijl, P. K., Brinkhuis, H., DeConto, R. M., Galeotti, S., Passchier, S., Pollard, D., Klaus, A., Fehr, A., Williams, T., Bendle, J. A. P., Bijl, P. K., Bohaty, S. M., Carr, S. A., Dunbar, R. B., Flores, J. A., Gonzàlez, J. J., Hayden, T. G., Iwai, M., Jimenez-Espejo, F. J., Katsuki, K., Kong, G. S., McKay, R. M., Nakai, M., Olney, M. P., Pekar, S. F., Pross, J., Riesselman, C., Röhl, U., Sakai, T., Shrivastava, P. K., Stickley, C. E., Sugisaki, S., Tauxe, L., Tuo, S., van de Flierdt, T., Welsh, K., and Yamane, M.: Relative sea-level rise around East Antarctica during Oligocene glaciation, Nat. Geosci., 6, 380–384, 2013. 3513, 3524

Tovchigrechko, A. and Vakser, I. A.: How common is the funnel–like energy landscape in protein–protein interactions?, Protein Sci., 10, 1572–1583, 2001. 3525

Tushingham, A. M. and Peltier, W. R.: Validation of the ICE-3G Model of Würm-Wisconsin Deglaciation using a global data base of relative sea level histories, J. Geophys. Res., 97, 3285–3304, 1992. 3524

Uppala, S. M., Kållberg, P. W., Simmons, A. J., Andrae, U., da Costa Bechtold, V., Fiorino, M., Gibson, J. K., Haseler, J., Hernandez, A., Kelly, G. A., Li, X., Onogi, K., Saarinen, S., Sokka, N., Allan, R. P., Andersson, E., Arpe, K., Balmaseda, M. A., Beljaars, A. C. M., van de Berg, L., Bidlot, J., Bormann, N., Caires, S., Chevallier, F., Dethof, A., Dragosavac, M., Fisher, M., Fuentes, M., Hagemann, S., Hólm, E., Hoskins, B. J., Isaksen, L., Janssen, P. A. E. M., Jenne, R., McNally, A. P., Mahfouf, J.-F., Morcrette, J.-J., Rayner, N. A., Saunders, R. W., Simon, P., Sterl, A., Trenberth, K. E., Untch, A., Vasiljevic, D., Viterbo, P., and Woollen, J.: The ERA-40 re-analysis, Q. J. Roy. Meteorol. Soc., 131, 2961–3012, 2005. 3512

van der Wal, W., Barnhoorn, A., Stocchi, P., Gradmann, S., Wu, P., Drury, M., and Vermeersen, B.: Glacial isostatic adjustment model with composite 3-D Earth rheology for Fennoscandia, Geophys. J. Int., 194, 61–77, 2013. 3524

Weber, M. E., Clark, P. U., Ricken, W., Mitrovica, J. X., Hostetler, S. W., and Kuhn, G.: Interhemispheric ice-sheet synchronicity during the Last Glacial Maximum, Science, 334, 1265–1269, 2011. 3510

Weertman, J.: Stability of the junction of an ice sheet and an ice shelf, J. Glaciol, 13, 3–11, 1974. 3510

Wessel, P. and Smith, W. H. F.: Free software helps map and display data, EOS, Transact. Am. Geophys. Union, 72, 441–441, 1991. 3515

Whitehouse, P. L., Bentley, M. J., and Le Brocq, A. M.: A deglacial model for Antarctica: geological constraints and glaciological modelling as a basis for a new model of Antarctic glacial isostatic adjustment, Quaternary Sci. Rev., 32, 1–24, 2012a. 3524

Whitehouse, P. L., Bentley, M. J., Milne, G. A., King, M. A., and Thomas, I. D.: A new glacial isostatic adjustment model for Antarctica: calibrated and tested using observations of relative sea-level change and present-day uplift rates, Geophys. J. Int., 190, 1464–1482, 2012b. 3524

Winkelmann, R., Martin, M. A., Haseloff, M., Albrecht, T., Bueler, E., Khroulev, C., and Levermann, A.: The Potsdam Parallel Ice Sheet Model (PISM-PIK) – Part 1: Model description, The Cryosphere, 5, 715–726, doi:10.5194/tc-5-715-2011, 2011. 3510

Woodward, R.: On the form and position of mean sea level, United States Geological Survey Bulletin, 48, 87–170, 1888. 3508

Yokoyama, Y., Lambeck, K., De Deckker, P., Johnston, P., and Fifield, L. K.: Timing of the Last Glacial Maximum from observed sea-level minima, Nature, 406, 713–716, 2000. 3507

Zweck, C. and Huybrechts, P.: Modeling of the Northern Hemisphere ice sheets during the last glacial cycle and glaciological sensitivity, J. Geophys. Res., 110, D07103, doi:10.1029/2004JD005489, 2005. 3509

Table 1. Separate model parameters for the four ice-sheet models.

Parameter	Description	EuIS	NaIS	GrIS	AIS
nx	ANICE x grid points	171	181	141	141
ny	ANICE y grid points	105	121	77	141
Δx	grid scale (km)	40	40	20	40
E_{ice}	SELEN elements	8766	7549	750	8947

Table 2. Example of pixels of the global mesh with the assigned values of the functions. OF: Ocean Function, FGI: Floating or Grounded Ice, AOF: Auxiliary Ocean Function (i.e. the time-dependent ocean function), m.s.l.: mean sea level.

	Lon (°E)	Lat (°N)	Topo (m)	OF	Ice (m)	FGI	AOF OF × FGI
(1) above m.s.l., ice–free	50.0	40.0	+250.0	0	0.0	1	0
(2) above m.s.l., ice–covered	320.0	70.0	+500.0	0	750.0	0	0
(3) below m.s.l., ice–free	50.0	40.0	−850.0	1	0.0	1	1
(4) below m.s.l., grounded ice	50.0	40.0	−100.0	1	550.0	0	0
(5) below m.s.l., floating ice	50.0	40.0	−350.0	1	50.0	1	1

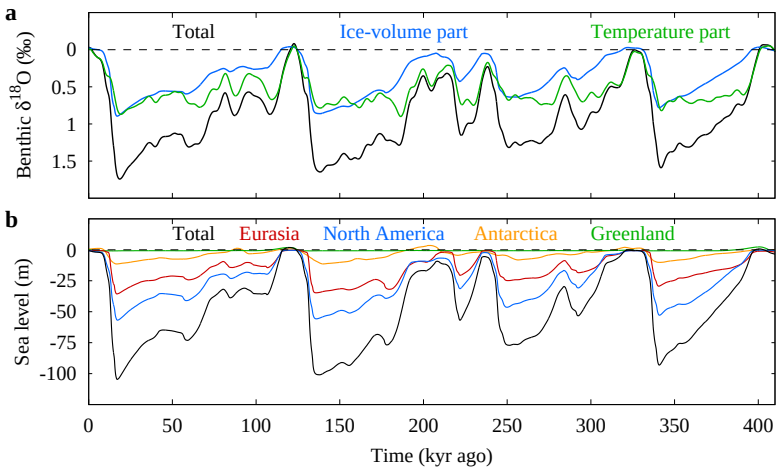

Figure 1. The uncoupled ANICE simulations using four ice-sheet-shelf models. **(a)** in black the LR04 (Lisiecki and Raymo, 2005) benthic δ^{18}O stack with the two separate contributions of ice volume (blue) and temperature (green). **(b)** The global eustatic sea level from ice volume in black with the four separate ice-sheet contributions of Eurasia (red), North America (blue), Antarctica (orange) and Greenland (green). Results are the same as shown in de Boer et al. (2014).

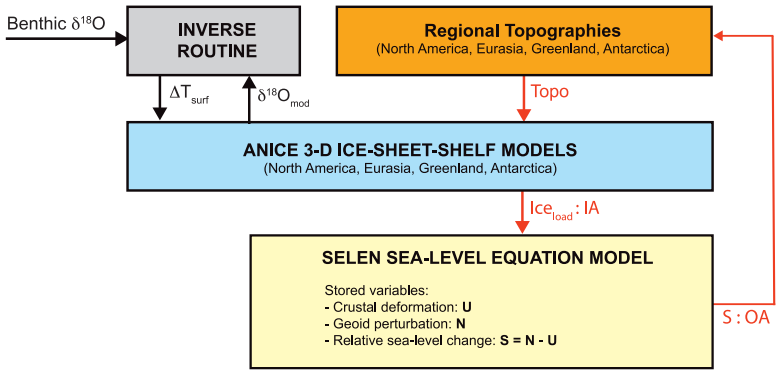

Figure 2. Scheme of the modelling framework. Black arrows indicate a coupling for every 100 years, red arrows show a coupling of every 1000 years. The model is forced with benthic δ^{18}O data, from which a temperature anomaly ΔT_{NH} is computed and forwarded to ANICE and the temperature module. ANICE is run for 100 years and computes the separate contributions of ice volume and temperature to benthic δ^{18}O. Every 1000 years ANICE forwards ice loading on land to SELEN, which computes the gravitationally self-consistent sea level and bedrock topography adjustment which are coupled back to ANICE.

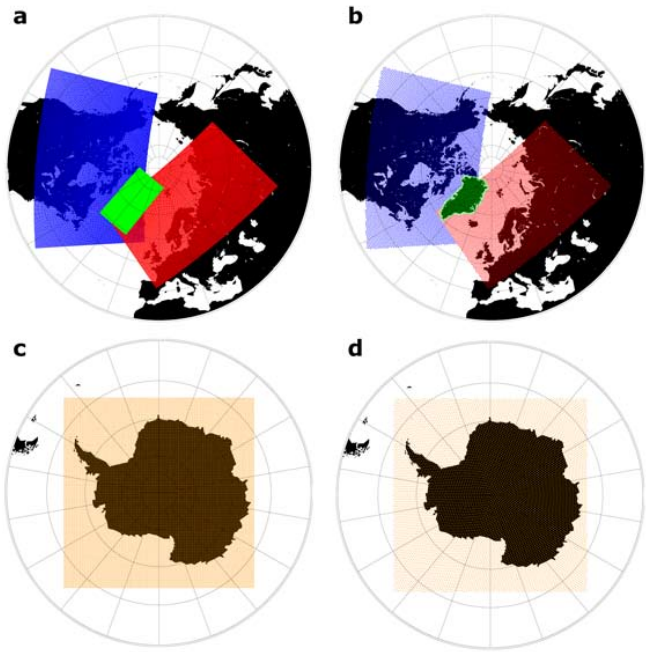

Figure 3. The four separate ANICE rectangular grid points for **(a)** the NH and **(c)** for Antarctica. The corresponding SELEN hexagonal elements for **(b)** the NH and **(d)** Antarctica. The colours correspond to each ice sheet. blue: NaIS, red: EuIS, green: GrIS and orange: AIS. the number of ANICE grid points and SELEN elements are shown in Table 1.

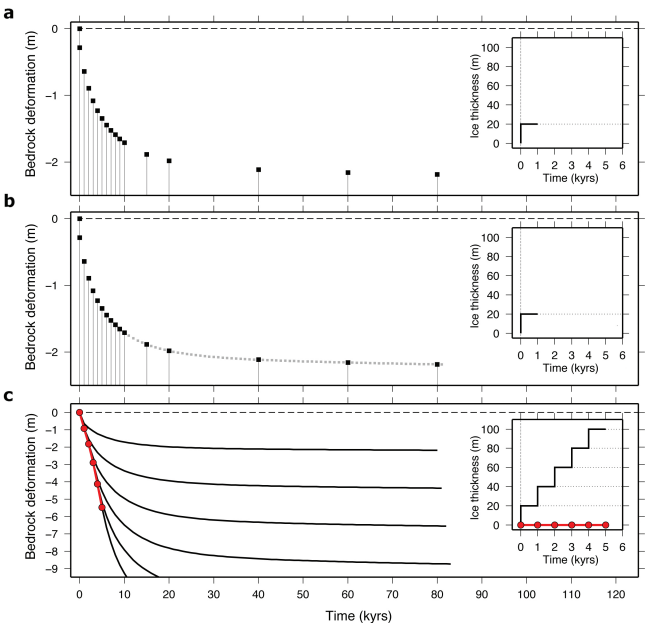

Figure 4. Bedrock deformation according to a sequential increase of ice thickness. Any 20 m increase of ice thickness contributes to 80 kyr of viscoelastic crustal deformation. **(a)** At t = 1 the predicted bedrock deformation at the 15 time steps of the moving time window. **(b)** Light grey markers indicate the fully discretised solution which is stored. **(c)** The predicted deformation for 5 consecutive time steps. The total solution, including past deformations is shown in red. Insets for **(a–c)** show the implied ice thickness variations, steps of 20 m per 1 kyr.

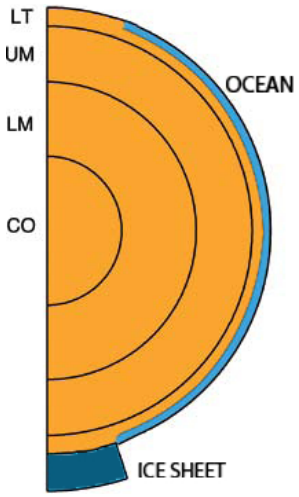

Figure 5. A slice of the schematic Earth used in the moving time window experiments. LT: Lithosphere of 100 km, UM: Upper mantle, a viscosity of 10^{21} Pa s, LM: Lower mantle: 2×10^{21} Pa s. CO: inviscid core.

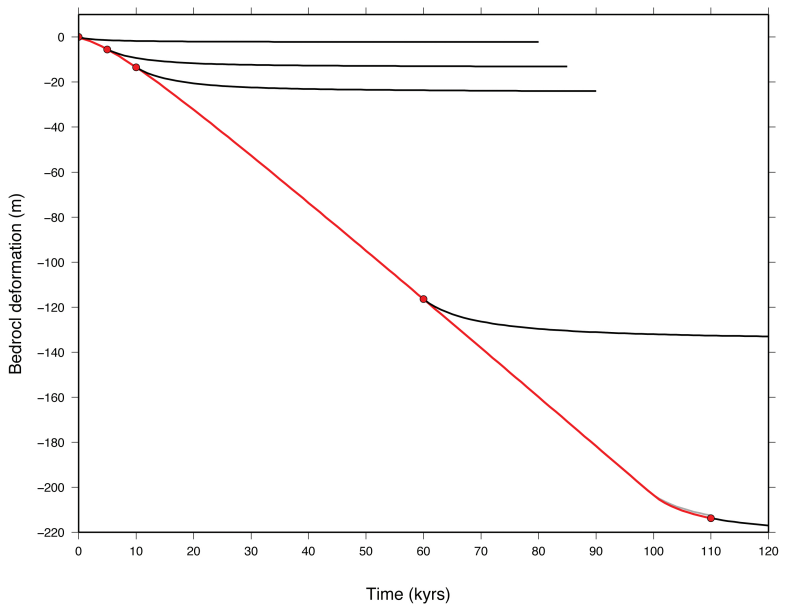

Figure 6. Predicted bedrock deformation through time according to the ice sheet thickness variation of 20 m per 1 kyr for a total of 110 kyr consecutive time steps, following the numerical scheme of Fig. 4. The black lines show the predicted deformation, stored in the memory, the red line is the full solution.

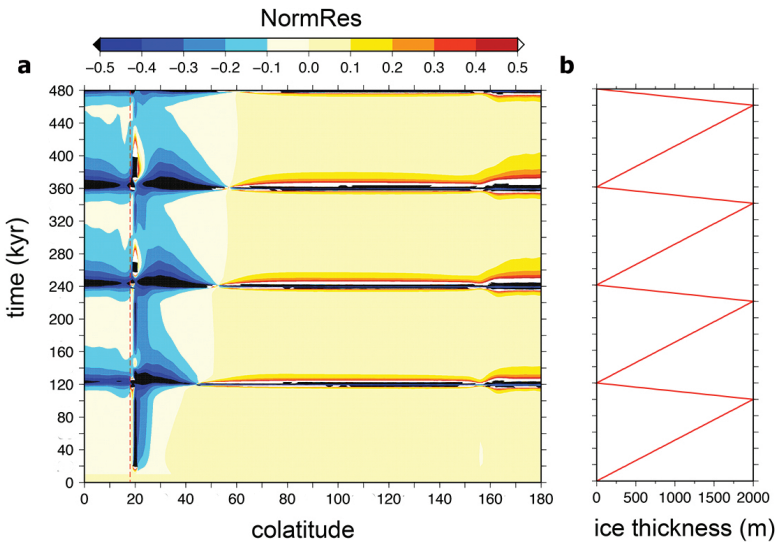

Figure 7. (a) Normalised residual of RSL change with the moving-time window relative to the standard SLE solution. Simulations are performed with a schematic Earth with two polar continents (Fig. 5), and an ice sheet on the south pole. The *y* axis shows the time, the *x* axis the co-latitude relative to the south pole. **(b)** Ice-thickness variation which is applied as a cylindrical shaped ice sheet up until 18° co-latitude (vertical red dashed line in **a**).

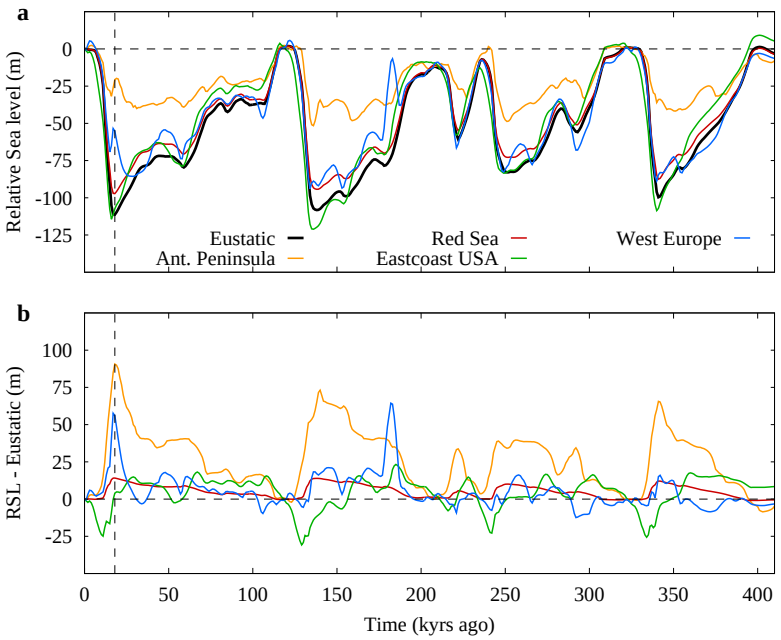

Figure 8. (a) RSL at four different locations. Red sea (red), Antarctic Peninsula (orange), West European coast (blue) and east coast of the USA (green). The black line indicates the eustatic RSL change. **(b)** RSL minus eustatic for each of the four locations.

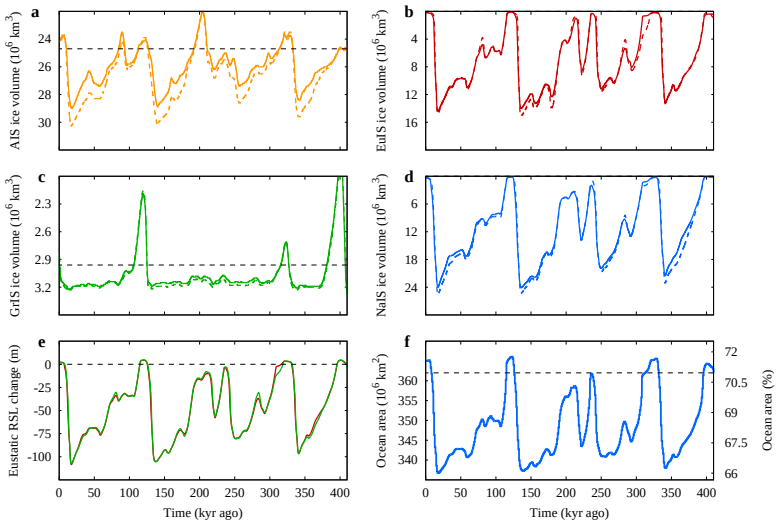

Figure 9. A comparison of the coupled ANICE-SELEN solution with model runs using the eustatic sea level. **(a)** The ice volume of the AIS, **(b)** Ice volume of the EuIS, **(c)** Ice volume of the GrIS and **(d)** ice volume of the NaIS. For all figures the coupled solution are shown by the solid line, the dashed line represents the model runs using the eustatic sea level (derived from ice volume as in de Boer et al., 2014). **(e)** The eustatic RSL change from the coupled run with SELEN in red and the eustatic sea level from de Boer et al. (2014) in green. **(f)** The evolution of the time dependent ocean function, on the left *y* axis the total ocean area, the right *y* axis show the percentage of ocean covered grid points over the globe.

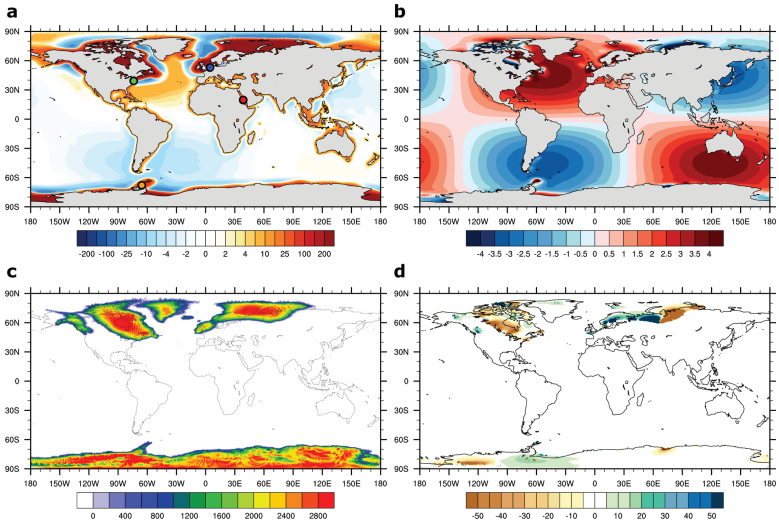

Figure 10. Results of a coupled ANICE-SELEN run at the Last Glacial Maximum (here 18 kyr ago). **(a)** RSL change with respect to the eustatic (= 111.3 m below PD) including rotational feedback. **(b)** The difference of RSL with a run without rotational feedback. **(c)** The total ice loading from ANICE (= 112.8 m s.e.) including rotational feedback. **(d)** The difference in ice loading with a run without rotational feedback. In **(a)** the coloured dots indicate the locations illustrated in Fig. 8.